JACS
JOURNAL OF THE AMERICAN CHEMICAL SOCIETY
Article
pubs.acs.org/JACS

Short-Axis Substitution Approach Selectively Optimizes Electrical Properties of Dibenzothiophene-Based Phosphine Oxide Hosts

Chunmiao Han,[†,‡] Zhensong Zhang,[§,‡] Hui Xu,[*,†] Shouzhen Yue,[§] Jing Li,[†] Pingrui Yan,[§] Zhaopeng Deng,[†] Yi Zhao,[*,§] Pengfei Yan,[†] and Shiyong Liu[§]

[†]Key Laboratory of Functional Inorganic Material Chemistry, Ministry of Education, Heilongjiang University, 74 Xuefu Road, Harbin 150080, P.R. China

[§]State Key Laboratory on Integrated Optoelectronics, College of Electronics Science and Engineering, Jilin University, 2699 Qianjin Street, Changchun 130012, P.R. China

Supporting Information

ABSTRACT: Two dibenzothiophene (**DBT**)-based phosphine oxide hosts, named 4-diphenylphosphoryl dibenzothiophene (**DBTSPO**) and 4,6-bis(diphenylphosphoryl) dibenzothiophene (**DBTDPO**), were prepared by short-axis substitution with the aim to selectively adjust electrical properties. The combined effects of short-axis substitution and the involvement of electron-donating S atom in conjugation effectively suppress the influence of electron-withdrawing diphenylphosphine oxide (DPPO) moieties on the frontier molecular orbitals and the optical properties. Therefore, **DBTSPO** and **DBTDPO** have the nearly same hole injection ability and the excited energy levels, while more electron-transporting DPPOs and the symmetrical configuration endow **DBTDPO** with enhanced electron-injecting/transporting ability. As the result, on the basis of this short-axis substitution effect, the selective adjustment of electrical properties was successfully realized. With the high first triplet energy level (T_1) of 2.90 eV, the suitable energy levels of the highest occupied molecular orbital and the lowest unoccupied molecular orbital of −6.05 and −2.50 eV and the improved carrier-transporting ability, **DBTDPO** supported its blue- and white-emitting phosphorescent organic light-emitting diodes as the best low-voltage-driving devices reported so far with the lowest driving voltages of 2.4 V for onset and <3.2 V at 1000 cd m^{-2} (for indoor lighting) accompanied with the high efficiencies of >30 lm W^{-1} and excellent efficiency stability.

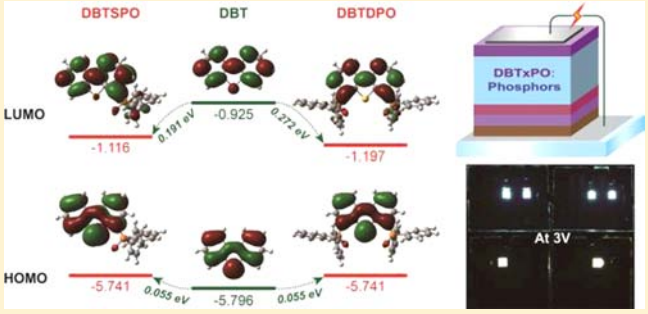

1. INTRODUCTION

After decades of development, organic optoelectronic materials have demonstrated their great potential in a number of applications, such as organic photovoltaics,[1] organic light-emitting diodes (OLEDs),[2−5] and sensors.[6] In recent years, the rising and urgent demand for high performances for commercial applications has driven persistent efforts to construct integrated systems with comprehensive and modified photoelectronic properties.[7−12] As a result, the contradictory between optical and electrical properties becomes more and more incisive. The origin of this issue is the common dependence of these properties (e.g., excited energy levels and charge injection ability) on molecular characteristics, especially the molecular energy levels. In this case, tuning one property often induces the simultaneous change of another one, which in turn induces an uncontrollable adjustment of material properties.[13−23] Therefore, the selective modulation of optoelectronic characteristics is still one of the biggest challenges in the field of high-performance organic optoelectronic materials. Nevertheless, we believe that modulation of a single property through one approach is more important than that of multiple properties, because it is much more operable to adjust the integral performance characteristics through purposeful and organizable modifications one by one. In this way, the uncontrollable interruptions between the approaches due to their overlapping effects can be avoided.

As a typical example, the contradiction between optical and electrical properties of host materials in blue-emitting phosphorescent organic light-emitting diodes (PHOLEDs)[24−28] is the sensitivity of both the singlet and triplet excited energy levels (S_1 and T_1) and the carrier injection/transporting ability to the functional substitution.[29] Active functional groups often simultaneously change the optical, carrier injection, and carrier-transporting performance of the materials.[30−33] In this situation, the high T_1 for exothermic energy transfer, suitable frontier molecular orbital (FMO) energy levels for carrier injection, and optimal molecular configuration and components for carrier transportation are hard to realize at the same time.[34] Therefore, although efforts have been undertaken to organize the optoelectronic properties of the hosts by integration of functional groups, only a few have

Received: August 20, 2012
Published: October 29, 2012

   dx.doi.org/10.1021/ja308273y | J. Am. Chem. Soc. 2012, 134, 19179−19188

achieved high electroluminescence (EL) efficiencies, such as external quantum efficiency (EQE) >10% and power efficiency (PE) >20 lm W^{-1}, accompanied by low driving voltages (e.g., <3 V for onset and <4V at 100 cd m^{-2} for portable display).[11,35−44] Thus, controllably modulating the optoelectronic properties of hosts is still one of the most significant issues in the development of efficient low-voltage driving PHOLEDs.

With the goal of alleviating the contradiction between optical and electrical properties and selective adjustment of specific properties, we constructed several ambipolar ternary fluorene-based hosts through indirect linkage to preserve the high T_1 of 3.0 eV.[37] Recently, we further designed a series of carbazole−phosphine oxide (PO) hybrids with dibenzofuran (**DBF**) bridges, whose FMOs and carrier injection/transporting abilities were continuously modified without influencing T_1. The extremely low driving voltages of 2.4 V for onset and 2.8 V at 100 cd m^{-2} were realized owing to the much improved hole injection/transportation by carbazolyls; however, the cost was an efficiency loss of 25−50%, compared with their parent molecules 4-diphenylphosphoryl dibenzofuran (**DBFSPO**)[39,40] and 4,6-bis(diphenylphosphoryl) dibenzofuran (**DBFDPO**).[45] Density functional theory (DFT) calculation showed that the electrostatic potential (ESP) distribution on **DBF** is not uniform due to the strong electronegativity of the O atom (Scheme 1), which enhances the stabilization ability of **DBF**

Scheme 1. ESP Distributions and Dipole Moments of DBTSPO and DBTDPO in Comparison to Their DBF-Based Analogues

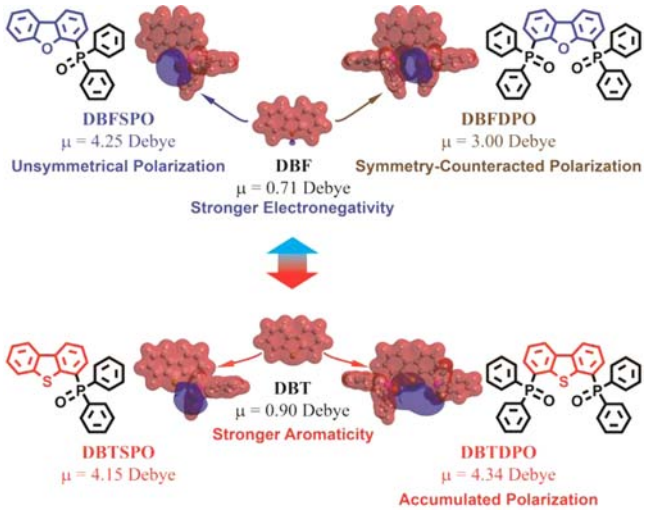

when an electron is injected. After substitution with diphenylphosphine oxide (DPPO) moieties, the negative charge is still located on this O atom, as well as O atoms in DPPOs. In this case, the preference of a **DBF** core for electron capture would be amplified to make the molecule more unipolar. Therefore, symmetrical substitution with two DPPOs instead reduces the dipole moment (μ) of **DBFDPO** to 3.00 D, compared with 4.25 D for unsymmetrical **DBFSPO**. This might be the main reason for the much higher driving voltages and reduced EL efficiencies of **DBFDPO**-based PHOLEDs.

In this contribution, we report two dibenzothiophene (**DBT**)-based PO hosts, namely 4-diphenylphosphoryl dibenzothiophene (**DBTSPO**) and 4,6-bis(diphenylphosphoryl) dibenzothiophene (**DBTDPO**), based on short-axis substitution to achieve highly efficient full-color PHOLEDs. An interesting effect of short-axis substitution on optoelectronic properties was discovered. As a result, we successfully and selectively improved the electron-injecting/transporting abilities with negligible influence on the optical properties and the highest occupied molecular orbital (HOMO) energy levels. Compared with **DBFDPO**-based devices, **DBTDPO** endows its blue- and white-emitting devices with the much higher efficiencies of ∼15% for EQE and >30 lm W^{-1} for PE, while their driving voltages are dramatically reduced to 2.4 V for onset, <2.8 V for 100 cd m^{-2}, and <3.2 V for 1000 cd m^{-2}. These ultralow operation voltages are even lower than the corresponding data for **DBF**-based donor−acceptor-type ambipolar PO hosts[46] and are the lowest reported so far among prototype blue- and white-emitting PHOLEDs.[29,47] The comprehensive EL performance indicates **DBTDPO** to be one of the best hosts reported so far for low-voltage driving of highly efficient PHOLEDs and demonstrates huge potential for use in portable energy-saving displays and lighting driven by low-voltage power sources.

2. RESULTS AND DISCUSSIONS

2.1. Design and Synthesis. It is known that although DPPO hardly changes excited energy levels owing to the insulating linkage of P═O, its electron-withdrawing characteristic results in a strong inductive effect. Commonly, for long-axis-substituted PO hosts, when the DPPO moieties in the molecules are increased, the HOMO and the lowest unoccupied molecular orbital (LUMO) energy levels are remarkably reduced by >0.2 eV at the same time.[48−52] However, our previous work indicated that short-axis substitution can reduce the influence of DPPO moieties on the HOMO.[39,45] Nevertheless, when the chromophore, such as **DBF**, is readily electron-transporting, short-axis substitution can still induce unipolarity of the molecules (Scheme 1). Therefore, in order to selectively tune a specific property of the host, the first step is to find a suitable chromophore with self-adaptability to modification.

It is recognized that **DBT** has a much stronger aromaticity than **DBF** owing to its much lower electronegativity and the involvement of an S atom in the conjugation. This is revealed by the uniform distribution of positive charge on the whole ring in ESP of **DBT** (Scheme 1). With the short-axis-substituted DPPOs, these two molecules can be efficiently polarized with the negative charge located on O atoms and positive charges on **DBT** and phenyls. In this case, the second DPPO, linked in the same direction, can further accumulate polarization of the disubstituted derivative. Therefore, **DBTDPO** has a bigger μ, 4.34 D, than **DBTSPO**, 4.15 D. In addition, substitution at the *ortho*-position may amplify the effects of the S atom by enhancing the electronic communication between the P and S atoms. This reflects the stability of the properties of short-axis-substituted **DBT**-PO derivatives and implies the potential for selective modulation of some specific properties.

DBTSPO and **DBTDPO** were conveniently prepared through a three-step procedure of regioselective lithiation, phosphorization, and oxidation, with moderate total yields of ∼60% and ∼30%, respectively (Scheme 2). The molecular structures of **DBTSPO** and **DBTDPO** were confirmed by single-crystal X-ray diffraction (XRD) analysis (Figure 1). Adjacent **DBTSPO** molecules were connected in a 1D chain structure through intermolecular C−H···π interactions (3.826 Å) along the *a* axis, as shown in Figure SI1a. It is noticed that

dx.doi.org/10.1021/ja308273y | J. Am. Chem. Soc. 2012, 134, 19179−19188

Scheme 2. Synthetic Route to DBTSPO and DBTDPO

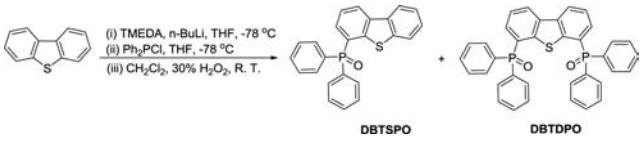

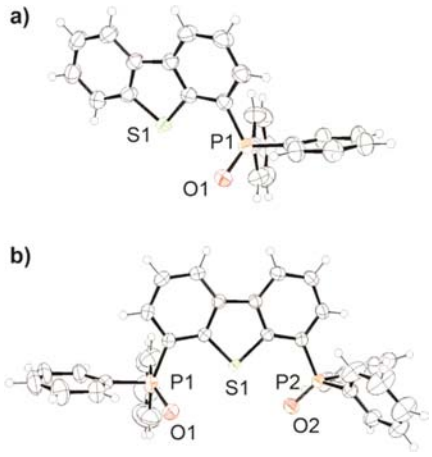

Figure 1. Single-crystal structures of **DBTSPO** (a) and **DBTDPO** (b).

there is no $\pi-\pi$ interaction with **DBT** in adjacent molecules. Furthermore, for **DBTDPO**, no intermolecular interactions are recognized except for van der Waals force (Figure SI1b). Therefore, DPPO moieties in the short-axis direction effectively suppress strong interactions, such as $\pi-\pi$ stacking. This is beneficial in that it reduces multiparticle quenching effects.[53−56] As the bridges formed between adjacent molecules, the effects of DPPOs on the intermolecular communications were amplified. The symmetrical configuration further endows **DBTDPO** with enhanced thermal and morphological stability. Its decomposition temperature (T_d = 442 °C) and glass transition temperature (T_g = 232 °C) are outstanding among the small molecular hosts (Figure SI2 and Table 1). The latter is improved by 126 °C compared with its 2,8-substituted analogue **PO15**,[57] owing to the more compact and rigid structure of the short-axis-substituted configuration. Atom force microscopy (AFM) and scanning electron microscopy (SEM) analyses of the vacuum-evaporated thin film of **DBTDPO** indicated a uniform amorphous state with root-mean-square roughness as small as 0.41 nm (Figure SI3). Obviously, the symmetrical and compact configuration of **DBTDPO** is beneficial to intermolecular arrangement, which induces the high film quality for nanometer-scale devices.

2.2. DFT Simulation and Electrical Properties. DFT calculation shows that the DPPO moiety in **DBFSPO** and **DBFDPO** can remarkably reduce the LUMO by ∼0.25 eV per DPPO (Figures 2 and SI4). However, their HOMOs also accordingly decrease by 0.12 eV. Obviously, the enhancement of electron injection ability of **DBFSPO** and **DBFDPO** is based on sacrificing partial hole injection ability, similar to some carbazole-based PO hosts.[50,58] Due to the strong electronegativity of the O atom in **DBF**, the HOMOs of the **DBF**-based molecules are localized on phenyls without the contribution of O atoms. This limited distribution decreases the HOMO energy levels. In contrast, the S atom in **DBT** contributes remarkably to the HOMO, so that the extensive conjugation results in its significantly higher HOMO energy level. The energy gap between the HOMOs of **DBF** and **DBT** reaches 0.19 eV (Figure 2). Nevertheless, DFT calculation of 2,8-substituted **DBT**-DPPO analogues (named **2-DBTSPO** and **2,8-DBTDPO**) showed that the *para*-substitution can still induce the simultaneous decrease of the LUMO and the HOMO of **DBT** cores (Figure SI5). As a result, the energy gap between FMOs of **DBT**, **2-DBTSPO** and **2,8-DBTDPO**, is nearly constant. The case is similar with **DBF**-based molecules. Inspiringly, as we expected, on the basis of short-axis substitution, **DBTSPO** and **DBTDPO** reveal excellent ability to adapt to the modifications. Even though 4-C and 6-C have remarkable contributions to the HOMOs, the substitution and the number of DPPO moieties have almost no influence on the HOMOs of **DBTSPO** and **DBTDPO**. With the small contributions by the S atoms, the LUMOs of **DBTSPO** and **DBTDPO** are reduced by the inductive effect of P═O by 0.19 and 0.27 eV, respectively. Therefore, the electron injection ability of **DBTSPO** and **DBTDPO** is improved without weakening their hole injection ability. The energy gaps of FMOs between **DBTSPO**/**DBFSPO** and **DBTDPO**/**DBFDPO** are ∼−0.1 eV for the LUMO and >0.4 eV for the HOMO, respectively, which reflects the comparable electron injection ability and much stronger hole injection ability of **DBTSPO** and **DBTDPO**. The smaller energy gap of **DBTDPO** than that of **DBTSPO** is also in accord with the results based on their dipole moments (Scheme 1). To figure out this unusual controllable modulation of molecular orbital energy levels, we further performed DFT calculations on *meta*-substituted **DBT**-DPPO analogues, named **3-DBTSPO** and **3,7-DBTDPO** (Figure SI5). Although the contributions of 3-C and 7-C to the FMOs of the molecules are almost negligible, the LUMOs and HOMOs of 3,7-substituted analogues are still much lower than those of **DBT**. As a result, only 4,6-substitution can suppress the influence of DPPO on the HOMOs. Obviously, this effect is related to the substitution

Table 1. Physical Properties of DBTSPO and DBTDPO

absorption peak (nm)	emission peak (nm)	S_1/T_1 (eV)	lifetime[a] (ns)	PLQY[a] (%)	HOMO/LUMO (eV)	T_d[h]/T_m/T_g (°C)
		DBTSPO				
332, 294, 284, 266, 238, 228[a]	363[a]	3.54[c]/2.98[d]	7.42	45.8	−5.741/−1.116[f]	342/226/−
297, 286, 253, 229[b]	364[b]	4.63[e]/3.10[e]			−6.05/−2.41[g]	
		DBTDPO				
340, 292, 288, 268, 251, 238[a]	363[a]	3.46[c]/2.90[d]	6.59	88.9	−5.741/ −1.197[f]	442/289/232
343, 301, 291, 268, 256, 249, 230[b]	364[b]	4.55[e]/3.35[e]			−6.05/−2.50[g]	

[a]In CH_2Cl_2, 1 × 10^{-6} mol L^{-1}. [b]In film. [c]Estimated from the absorption edge. [d]Estimated from the first triplet transition peak. [e]Results of DFT calculation. [f]According to DFT calculation. [g]Calculated with the onset potentials of the redox peaks in the cyclic voltammogram. [h]At 5% weight loss.

dx.doi.org/10.1021/ja308273y | J. Am. Chem. Soc. 2012, 134, 19179−19188

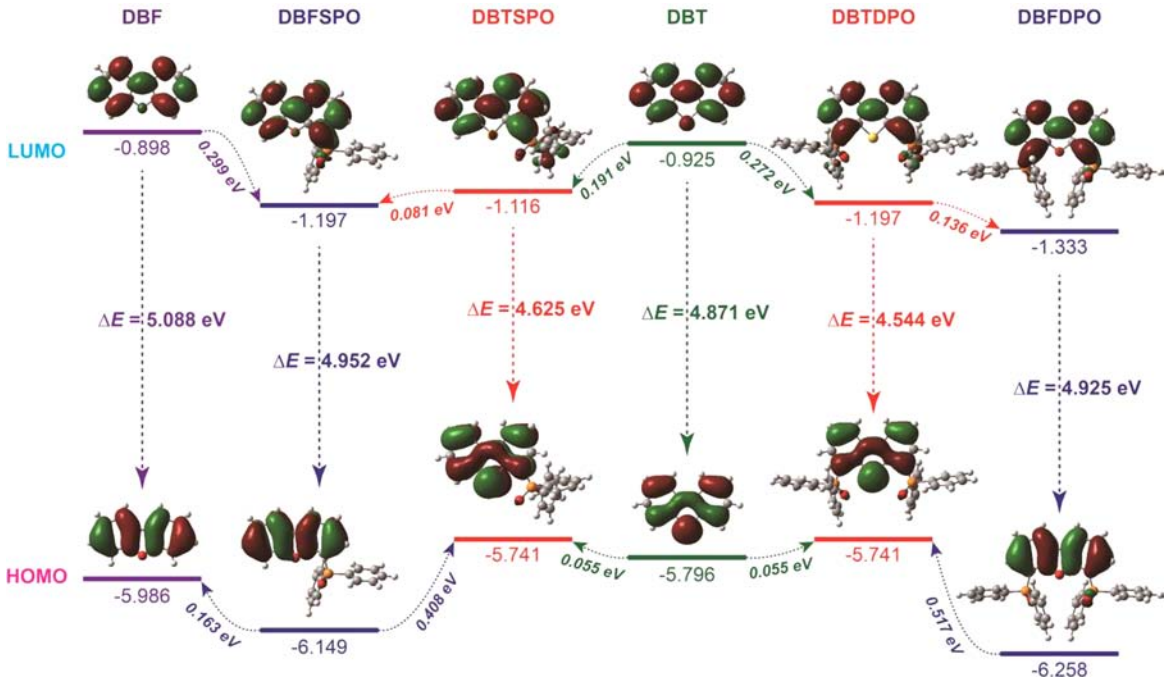

Figure 2. Energy level scheme of FMOs of DBF and DBT derivatives according to DFT calculation.

position and the hetero atoms in the chromophore rings. Aside from the weaker electronegativity, the S atom in **DBT** has 3p lone-pair electrons with much larger scope than that of 2p lone-pair electrons of the O atom in **DBF**. In this sense, the potential electron communications between the S atom and *ortho*-substituted DPPO moieties in **DBTSPO** and **DBTDPO** might be more effective. Closer observation of the LUMO electron cloud distributions indicates that, compared with **DBT**, the contribution of the S atom in **DBTSPO** to the LUMO is much reduced, and the S atom in **DBTDPO** is hardly involved in the LUMO. This situation is just the reverse of that of their *para*- and *meta*-substituted analogues, for which the contributions of their S atoms to the LUMO are almost unchanged after DPPO modification (Figure SI5). Since the distances between S and P atoms in **DBTSPO** and **DBTDPO** are ∼3.4 Å, much longer than the common P═S bond length of ∼1.95 Å, the electron communication between them cannot form substantive P═S bonds. It might be a kind of long-range interaction similar to back-bonding,[59] which strongly polarizes S atoms and consequently results in their non-involvement in LUMO. Comparison of single-crystal structure data of **DBTSPO**, **DBTDPO**, **DBFSPO**,[39] and **DBFDPO**[45] gives direct evidence. The lengths of C−P bonds in **DBFSPO** and **DBFDPO** are 1.79−1.81 Å, similar to the common C−P bond length of PO compounds reported previously.[59] However, for **DBTSPO** and **DBTDPO**, the lengths of C−P bonds adjacent to S atoms increase by 0.001−0.01 Å. Since the C−P bond length in known phosphine sulfide compounds is 1.81−1.82 Å,[59] the elongation of C−P in **DBTSPO** and **DBTDPO** further directs the influence of 3p lone-pair electrons of the S atom on the P atom, similar to back-bonding effect. For further comparison, DFT calculations of **DBT** analogues with two different electron-withdrawing substituents, F atom and nitro group, without back-bonding effect were also performed (Figure SI6). The remarkable reduction of the HOMOs in these molecules is almost unrelated to the substitution position. Therefore, we think at least one of the main reasons for this selective FMO tuning is the electronic communication between S and P atoms on the basis of short-axis substitution. This is a brand-new effect, named the short-axis substitution effect, discovered for controllable tuning of molecular orbitals, which can further guide the design of the *third and later row* elements involved in functional conjugated systems. DFT calculation indicates that the *ortho*-substituted DPPO hardly influences T_1 states of **DBTSPO** and **DBTDPO**, at ∼3.1 eV, which is ascribed to the predominant contribution of **DBT** to T_1 states as shown by the localized spin densities of their T_1 states on **DBT**s (Figure SI7).

The electrochemical analysis presented direct experimental evidence for the short-axis substitution effect (Figure 3). The cyclic voltammograms of **DBTSPO** and **DBTDPO** showed irreversible oxidation peaks with exactly the same turn-on voltage of 1.65 V, corresponding to a HOMO energy level of −6.05 eV, while the turn-on voltages of the irreversible oxidation peaks of the **DBF**-based analogues were 1.77 and 1.89

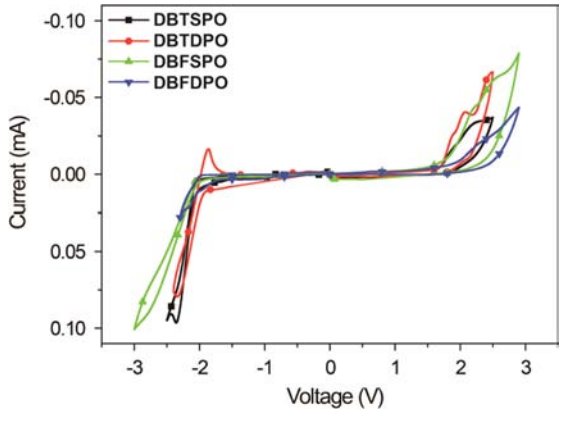

Figure 3. Cyclic voltammograms of **DBTSPO** and **DBTDPO**. The measurement was performed in tetrahydrofuran and dichloromethane, respectively, with tetrabutylammonium hexafluorophosphate as electrolyte at room temperature and a rate of 100 mV s^{-1}.

dx.doi.org/10.1021/ja308273y | J. Am. Chem. Soc. 2012, 134, 19179−19188

eV, corresponding to HOMO energy levels of −6.17 and −6.29 eV, respectively. **DBTSPO**, **DBFSPO**, and **DBFDPO** have irreversible reduction peaks with turn-on voltages of −1.99, −1.99, and −1.75 V, corresponding to LUMO energy levels of −2.41, −2.41, and −2.65 eV, respectively. **DBTDPO** showed a reversible reduction peak with the turn-on voltage of −1.90 V, corresponding to a LUMO energy level of −2.50 eV. These results are exactly in accord with DFT calculation. The HOMOs of **DBTSPO** and **DBTDPO** are 0.12 and 0.24 eV higher than those of **DBFSPO** and **DBFDPO**, respectively. However, **DBTSPO** and **DBFSPO** have the same LUMO energy levels, and the LUMO energy levels of **DBTDPO** and **DBFDPO** are similar. The second DPPO moiety has no influence on the HOMO of **DBTDPO** but decreases its LUMO. Therefore, the improved electron injection ability is achieved with preservation of original hole injection ability.

We further investigated the carrier-transporting ability of these materials through their nominal hole-only and electron-only devices (Figure 4). The hole-only and electron-only

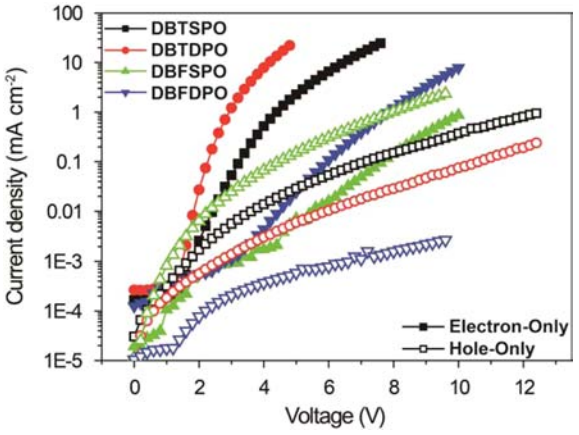

Figure 4. *I*−*V* characteristic curves of single-carrier-transporting devices based on **DBTSPO** and **DBTDPO**.

devices were fabricated with the structures of ITO|MoO_x (2 nm)|*m*-MTDATA:MoO_x (15 wt%, 30 nm)|*m*-MTDATA (10 nm)|$Ir(ppz)_3$ (10 nm)|**PO Host** (30 nm)|$Ir(ppz)_3$ (10 nm)|*m*-MTDATA (10 nm)|*m*-MTDATA:MoO_x (15 wt%, 30 nm)|MoO_3 (2 nm)|Al and ITO|Cs_2CO_3 (1 nm)|BPhen (40 nm)|**PO Host** (30 nm)|BPhen (40 nm)|Cs_2CO_3 (1 nm)|Al, respectively, where MoO_x and Cs_2CO_3 served as hole- and electron-injecting layers, *m*-MTDATA is 4,4′,4″-tris(*N*-3-methylphenyl-*N*-phenylamino)triphenylamine as the hole-transporting layer, $Ir(ppz)_3$ is tris(phenylpyrazole)iridium as hole-transporting/electron-blocking layer, and BPhen is 4,7-diphenyl-1,10-phenanthroline as electron-transporting/hole-blocking layer. The electron-only current densities (*J*) of **DBTSPO** and **DBTDPO** were much bigger than their hole-only *J*, which indicated predominant electron transport in **DBTSPO** and **DBTDPO**. It is also noticed that the electron-transporting ability of **DBTDPO** is stronger than that of **DBTSPO** by an order of magnitude, while for the hole-transporting ability the situation is precisely the opposite. According to DFT calculations, both holes and electrons are readily injected in **DBT** cores, which are separated by DPPO moieties. Therefore, **DBTSPO** is superior in hole transportation with the smaller interference by its less pendent DPPO moiety. However, DPPOs can facilitate intermolecular electron transport originating from their contributions to unoccupied molecular orbitals (LUMO+1 for **DBTSPO**; LUMO+1 and LUMO+2 for **DBTDPO**). The more and symmetrically substituted DPPO moieties in **DBTDPO** provide much more efficient electron transport than that in **DBTSPO**. The electron-transporting characteristic of DPPOs is also the main reason for the predominant electron transport in both **DBTSPO** and **DBTDPO**. It is noticeable that, compared with **DBFSPO**, the enhancement of electron-transporting ability of **DBFDPO** is based on the much more remarkable reduction in its hole-transporting ability. **DBTDPO** is distinctly superior to **DBFDPO** in carrier transportation. Although the hole-transporting ability of **DBTDPO** is weaker than that of **DBTSPO**, the superiority of the former in electron transport is more conspicuous. **DBTSPO** exhibited the more balanced carrier-transporting ability; however, among these four PO hosts, **DBTDPO** exhibits the strongest electron-transporting ability, accompanied by moderate hole-transporting ability. Obviously, the advantages of **DBTDPO** in carrier injection and transportation establish a solid basis for their use in low-voltage driving devices.

2.3. Optical Properties. The absorption spectra of **DBTSPO** and **DBTDPO** (in dilute CH_2Cl_2 solutions (1×10^{-6} mol L^{-1})) are nearly the same (Figure 5 and Table 1),

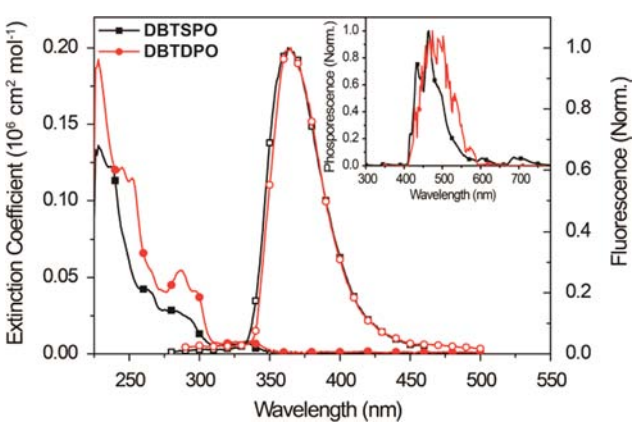

Figure 5. Absorption, fluorescence, and phosphorescence (inset) spectra of **DBTSPO** and **DBTDPO** in dichloromethane (1×10^{-6} mol L^{-1}). The excitation wavelength was 250 and 280 nm for **DBTSPO** and **DBTDPO**, respectively. Absorption and fluorescence spectra were measured at room temperature. Phosphorescence spectra were recorded at 77 K with a delay of 300 μs.

composed of four bands at 315−350 nm (n→π^* transition of **DBT**), 275−315 nm (π→π^* transition of **DBT**), 235−270 nm (π→π^* transition from DPPO to **DBT**), and 225−235 nm (π→π^* transition of DPPO). The larger absorption cross section of **DBTDPO** induces its bigger extinction coefficient. S_1 values of **DBTSPO** and **DBTDPO** are estimated as 3.54 and 3.46 eV according to their absorption edges at 350 and 358 nm, respectively. Their close S_1 values are in accord with their similar HOMO−LUMO energy gaps by DFT calculation (Figure 2). The fluorescent emissions of **DBTSPO** and **DBTDPO** (1×10^{-6} mol L^{-1} in CH_2Cl_2 at room temperature) are also nearly the same in shape and emission peak (at 363 nm), which are ascribed to the radiative π^*→n transition of **DBT** cores. Furthermore, no bathochromic shift was observed in their emission spectra in various solvents with different polarities (Figure SI8). This indicates the suppressed charge transfer between **DBT** cores and DPPOs through the short-axis

dx.doi.org/10.1021/ja308273y | *J. Am. Chem. Soc.* 2012, 134, 19179−19188

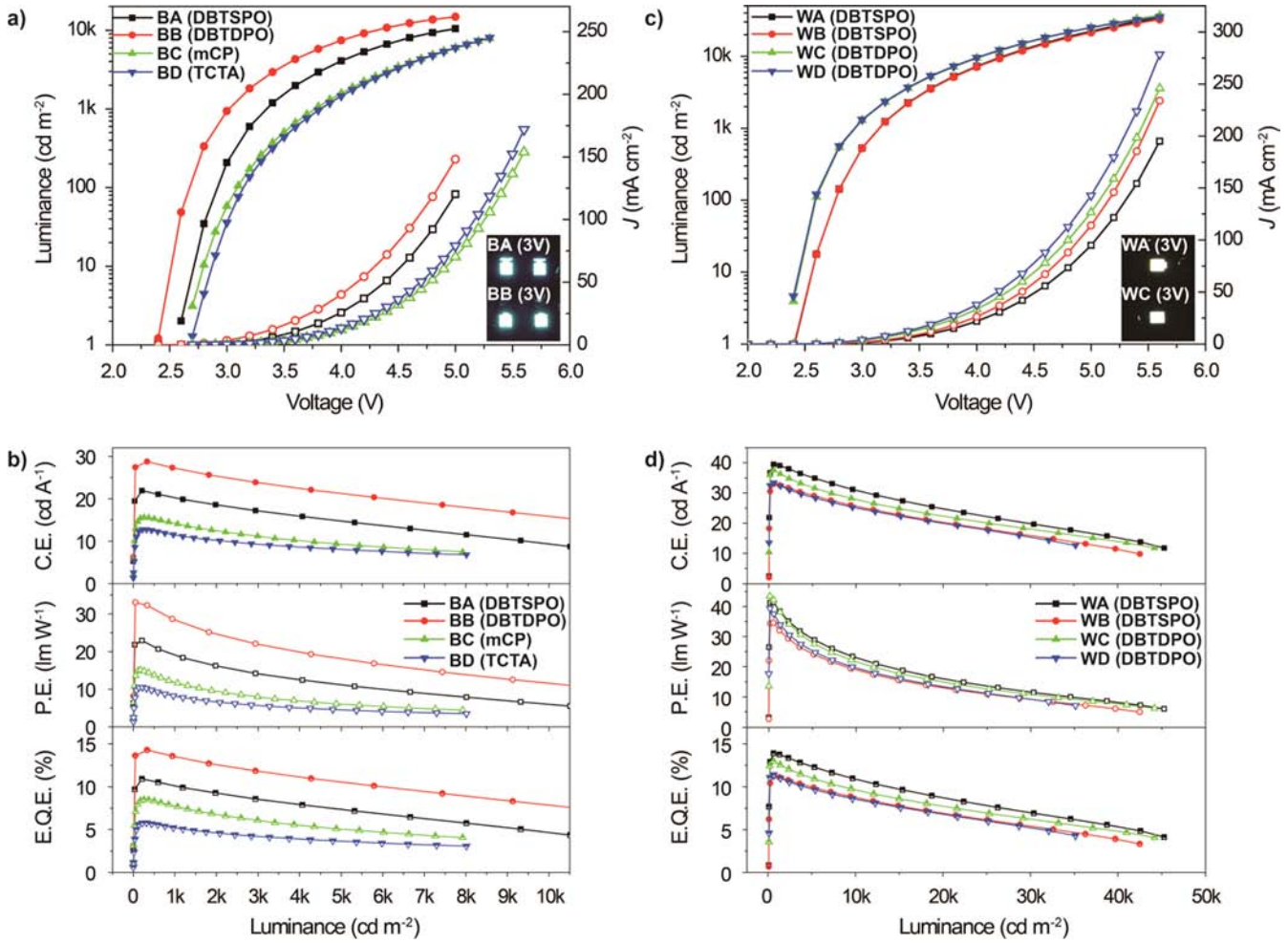

Figure 6. Brightness–current density (J)–voltage curves (a,c) and efficiency–brightness curves (b,d) of blue- and white-emitting PHOLEDs based on **DBTSPO** and **DBTDPO**.

substitution. The absorption and emission spectra of **DBTSPO** and **DBTDPO** in film are similar with their spectra in solution (Figure SI9). The preserved fine structures of absorption bands, the stable emission peaks at 364 nm, and the narrow emissions with full widths at half-maximum of <55 nm revealed their weak intermolecular interaction. The time-resolved phosphorescence spectra of **DBTSPO** and **DBTDPO** in CH_2Cl_2 glass at 77 K were measured to determine their T_1 values. Their 0–0 transition bands are at 416 and 428 nm, corresponding to T_1 = 2.98 and 2.90 eV, respectively, which are high enough for the exothermic energy transfer to blue phosphors.

It is obvious that the short-axis substitution effect selectively suppresses the influence of DPPOs on the optoelectronic properties of **DBTSPO** and **DBTDPO**. Therefore, they exhibit similar HOMO energy levels and excited energy levels. Furthermore, the distinctions in molecular symmetry and number of electron-transporting DPPOs result in different carrier-transporting abilities of **DBTSPO** and **DBTDPO**. In this sense, we successfully and selectively enhanced the electron-injecting/transporting ability of **DBTSPO** and **DBTDPO** with only small influences on other optoelectronic properties. **DBTSPO** and **DBTDPO** actually provide a perfect platform to investigate the influence of carrier-injecting/transporting ability of the hosts on the EL performance of PHOLEDs.

2.4. EL Performance of PHOLEDs. To clarify the effect of selective modification of electrical properties on improving EL performance, the blue-emitting devices **BA** and **BB** were fabricated with the general configuration of ITO|MoO_x (2 nm)|*m*-MTDATA:MoO_x (15 wt%, 30 nm)|*m*-MTDATA (10 nm)|$Ir(ppz)_3$ (10 nm)|**Host**:Dopants (10 nm, 10%)|BPhen (40 nm)|Cs_2CO_3 (1 nm)|Al, in which bis[2-(4,6-difluorophenyl)-pyridinato-*N*,C^2]picolinate iridium(III) (FIrpic) was used as blue-emitting dopant. **DBTSPO** and **DBTDPO** served as host in **BA** and **BB**, respectively (Scheme SI1). The most common hosts for PHOLEDs, namely tris(4-(9*H*-carbazol-9-yl)phenyl)-amine and *N*,*N*-dicarbazolyl-3,5-benzene, were also used to fabricate devices **BC** and **BD** for comparison. The driving voltages of **BA** were 2.6 V for onset, <3.0 V (100 cd m^{-2}), <3.4 V (1000 cd m^{-2}), and <5.0 V (10 000 cd m^{-2}), respectively, which were lower than those of **BC** and **BD** (2.7 V for onset, ~3.2 V at 100 cd m^{-2}, and ~3.8 V at 1000 cd m^{-2}) (Figure 6a). Inspiringly, the most electron-transporting **DBTDPO** endowed **BB** with the extremely low driving voltages of 2.4 V for onset, < 2.8 V for 100 m^{-2} (333 cd m^{-2}), < 3.2 V for 1000 cd m^{-2} (1819 cd m^{-2}), and <4.4 V for 10 000 cd m^{-2} (10 800 cd m^{-2}), respectively. To the best of our knowledge, these are the lowest driving voltages reported so far for the blue-emitting PHOLEDs with the prototype device configurations.[29] Furthermore, the driving voltage at 1000 cd m^{-2} of **BB** was

dx.doi.org/10.1021/ja308273y | *J. Am. Chem. Soc.* 2012, 134, 19179–19188

dramatically reduced by ~1 V compared with similar devices of **DBFSPO** (Table SI1).

Along with the ultralow driving voltages, high and stable efficiencies were also achieved by **BA** and **BB**. The maximum efficiencies of **BA** reached 21.9 cd A^{-1} for current efficiency (CE), 22.9 lm W^{-1} for PE, and 10.9% for EQE, which were much higher than those of **BC** and **BD** (Figure 6b). **BB** realized the largest efficiencies among these blue-emitting devices, its maximum efficiencies being as high as 28.8 cd A^{-1}, 33.1 lm W^{-1}, and 14.3%, which make **BB** favorable among the most efficient blue-emitting devices reported so far.[29,47] The ultralow driving voltages of **BA** and **BB** made their PE bigger than CE, which is unusual for blue PHOLEDs and reveals their advantage in energy conservation. **BA** and **BB** also exhibited the stable efficiencies, in that at 1000 cd m^{-2} their efficiency roll-offs were only 9.6% CE, 22.1% PE, and 9.2% EQE for **BA** and 5.2% CE, 13.6% PE ,and 4.9% EQE for **BB**. It is noticed that **BB** showed much better performance than **BA** owing to the stronger electron-transporting ability and preserved hole-injecting/transporting ability of **DBTDPO**. The suppressed influences of DPPO on optoelectronic properties by the unique short-axis substitution effect make the EL performance of **DBTSPO** and **DBTDPO** opposite to that of their **DBF**-based analogues (Table SI1). The efficiencies of **BB** were similar to those of **DBFSPO**-based devices, while **BB** was superior with much lower operating voltages. This result directly demonstrates the superiority of selective modulation in accurate optimization of optoelectronic properties.

We also fabricated the green (**G**)-, yellow (**Y**)-, and red (**R**)-emitting PHOLEDs with the general configuration based on tris(2-phenylpyridine) iridium(III) ($Ir(ppy)_3$), bis(2-phenylbenzothiazolato)(acetylacetonate) iridium(III) ($Ir(bt)_2acac$), and bis(2-methyldibenzo[*f*,*h*]quinoxaline)(acetylacetonate) iridium(III) ($Ir(MDQ)_2acac$), respectively, with the corresponding concentrations of 8, 6, and 10%. **GA**, **YA**, and **RA** used **DBTSPO** as host, while **GB**, **YB**, and **RB** were based on **DBTDPO** (Scheme SI1). **DBTDPO** endowed its devices with the extremely low driving voltages of ≤2.6 V for onset and <3.2 V at 100 cd m^{-2} for display, which were generally 0.2 V lower than those of **DBTSPO**-based devices (Figure SI11 and Table SI2). However, at voltages >4.0 V, the brightness of **GA** and **YA** gradually exceeded that of **GB** and **YB**. This implied worse quenching in these **DBTDPO**-based devices. As distinct evidence, for the **G**- and **Y**-emitting devices, **DBTSPO** supported higher maximum efficiencies and efficiency stabilities than **DBTDPO**. In addition, although the maximum efficiencies of **RB** were higher than those of **RA**, the former still revealed much sharper efficiency reduction at high luminance. Since the optical properties of these two **DBT**-based PO hosts are similar, the worse emission quenching in EMLs of small energy-gap phosphors-doped **DBTDPO** should be attributed to the mismatch of carrier-injecting/transporting ability between the host and dopants. The extremely strong electron transport provided by **DBTDPO** induced excessive accumulation of excitons at the interfaces between electron-blocking $Ir(ppz)_3$ and EMLs, which worsened the multiparticle quenching effects.[55,56] Nevertheless, both **DBTSPO** and **DBTDPO** realized the high-performance green, yellow, and red PHOLEDs with low driving voltages and high efficiencies.

The excellent monochromic PHOLEDs inspired us to further investigate the performance of **DBTSPO** and **DBTDPO** as the single host for white-emitting PHOLEDs (WPHOLEDs), namely **WA** and **WC** with the general configuration (except for their dual EMLs) of **Host**:FIrpic (10 wt%, 4 nm)|**Host**:iridium(III) bis(4-phenylthieno[3,2-*c*]pyridinato-*N*,C^2) acetylacetonate (PO-01) (6 wt%, 6 nm), respectively. The white emission was achieved through the mixture of complementary blue (from FIrpic) and yellow (from PO-01) lights. The ultralow driving voltages were also inherited for **WC** (Figure 6c and Table SI1). The luminance >1000 cd m^{-2} for indoor lighting and 10 000 cd m^{-2} for outdoor lighting was realized at as low as 3.0 (1294 cd m^{-2}) and 4.2 V (12 010 cd m^{-2}) with small current density (*J*) of 3.6 and 45.3 mA cm^{-2}, which can be easily afforded by commercial lithium ion batteries (4.2 V, 1200 mAh). Therefore, **WC** is suitable and feasible for use in portable light sources, such as tactical spotlights, signal lamps, and cap-lamps. It can also be integrated in portable digital devices, e.g., mobile phones, as backlight for active matrix displays and emergency lighting. The driving voltages of **WA** were ~0.2 V higher than those of **WC** at the same luminance, due to the inferior electron injection and transportation in **DBTSPO**. Nevertheless, **WA** can still be competent for portable applications.

Because of the predominant contribution of yellow in complementary-color white light, the better fitness of **DBTSPO** to yellow phosphors endowed **WA** with slightly higher maximum CE and EQE (39.6 cd A^{-1} and 13.9%) than those of **WC** (37.6 cd A^{-1} and 13.0%), even though the lower driving voltage supported a higher maximum PE of **WC** (43.5 lm W^{-1}) than that of **WA** (41.2 lm W^{-1}) (Figure 6d and Table SI1). Both **WA** and **WC** showed such extremely high efficiency stability that at 1000 cd m^{-2} the efficiency roll-offs of **WA** were only 1% CE, 7% PE, and 1% EQE, respectively, which were less than half those of **DBFSPO**-based WPHOLEDs. At 5000 cd m^{-2}, the roll-offs of **WA** were still well controlled,with 12% CE, 30% PE, and 12% EQE. The efficiency roll-offs of **WC** were slightly bigger: 3, 12, and 3% at 1000 cd m^{-2} and 16, 37, and 16% at 5000 cd m^{-2} in the order of CE, PE, and EQE. Compared with **DBFSPO**-based WPHOLEDs, PEs of **WA** and **WC** were improved by 15%, accompanied by their reduced roll-offs. Through additional luminance enhancement with micro-lens outcoupling, their PE at 1000 cd m^{-2} can approach 80 lm W^{-1}. Therefore, **DBTSPO** and **DBTDPO** endowed their single-host WPHOLEDs with high performance comparable to the best reports of multihost WPHOLEDs.[60]

The EL spectrum of **WA** at 1000 cd m^{-2} showed warm white emission with a correlated color temperature (CCT) of 4138 K, while the more remarkable contribution of the blue portion in the EL spectrum of **WC** resulted in a higher CCT of 4983 K (Figure SI12). The different EL spectra of **WA** and **WC** should be attributed to the variation of exciton recombination zones. The yellow emission in these devices was generated through two channels: direct recombination in the PO-01 layer and exciton diffusion from the FIrpic layer. Since the thickness of the FIrpic layer is only 4 nm to support efficient energy transfer to the PO-01 layer, the stronger blue emission of **WC** implied that its recombination zone should be definitely located in the FIrpic layer. To figure out this issue, we fabricated two other devices, **WB** and **WD**, of **DBTSPO** and **DBTDPO** with the position-interchanged dual EMLs of **Host**:PO-01 (6 wt%, 4 nm)|**Host**:FIrpic (10 wt%, 6 nm). Only yellow emissions from PO-01 can be recognized in EL spectra of **WD** (Figure SI12). The absence of blue emission clearly indicated that the strong electron-transporting ability of **DBTDPO** limited the exiton recombination to a narrow zone of <4 nm at the interface between the $Ir(ppz)_3$ layer and EMLs. In contrast, weak but

dx.doi.org/10.1021/ja308273y | *J. Am. Chem. Soc.* 2012, 134, 19179−19188

distinct blue emissions were observed in EL spectra of **WB**. In comparison with **WA**, the smaller blue contribution in EL spectra of **WB** points out that their exciton recombination zones were at the interface between two EMLs and majorly located in the one adjacent to the $Ir(ppz)_3$ layer. This should be due to the more balanced carrier-injecting/transporting ability of **DBTSPO**. Therefore, **WA** and **WB** were superior in wide emission zones to suppress the concentration quenching effect and multiparticle annihilation processes. This should be the main reason for the slightly higher efficiencies and efficiency stability of **WA**. We also noticed that the brightness and efficiencies of **WA** were much higher than those of **BA**. This should be due to the efficient utilization of excessive excitons in FIrpic layers through exciton diffusion. To demonstrate it, we fabricated another **WA**-type device but with equal thicknesses of the dual EMLs of 5 nm. The proportion of blue emission became much bigger. The maximum luminance was reduced to <30 000 cd m^{-2}, accompanied by the smaller efficiency of 32 cd A^{-1}. This is obviously ascribed to the 1 nm longer exciton diffusion distance from the exciton recombination zone to the PO-01 layer. The longer exciton diffusion distance for **WC** should be another main reason for its smaller efficiencies and bigger roll-off than those of **WA**.

The well-controlled electrical properties of **DBTSPO** and **DBTDPO** were dramatically presented through their high-performance PHOLEDs. The investigation clearly reflects the direct relationships between the carrier-injecting/transporting ability of the hosts and the driving voltages, efficiencies, and roll-offs of the devices. Therefore, the purposeful and selective modulation of optoelectronic properties can rationally improve the corresponding performance of the devices. Table SI1 makes the comparison between EL performance of several representative hosts for blue- and white-emitting PHOLEDs. It is noteworthy that **DBTSPO** and **DBTDPO** not only supported their devices with the lowest driving voltages but also achieved favorable efficiencies. Owing to their advantages in reducing operation voltage, their WPHOLEDs were outstanding in energy conservation, with PE >40 lm W^{-1}. The state-of-the-art performance makes **DBTSPO** and **DBTDPO** among the best hosts for blue- and white-emitting PHOLEDs reported so far.[29]

3. CONCLUSIONS

We selectively and effectively suppressed the negative influence of electron-withdrawing DPPO groups on the optoelectronic properties of two **DBT**-based PO hosts, **DBTSPO** and **DBTDPO**, with a unique short-axis substitution effect. **DBTSPO** and **DBTDPO** reveal almost the same hole injection ability and optical properties with similar HOMO energy levels and excited energy levels. However, differences in the molecular symmetry and the number of electron-transporting DPPO groups result in the distinct electron-injecting/transporting abilities of **DBTSPO** and **DBTDPO**. This controllable modulation endowed **DBTDPO** with the comprehensive properties of stronger electron-injecting/transporting ability without interference in hole injection/transportation and T_1. Therefore, selective modification of electron injection and transportation without changing other optoelectronic properties was successfully realized. The corresponding blue and white PHOLEDs based on **DBTDPO** showed excellent performance, including driving voltages of <2.8 V for 100 cd m^{-2} and 3.2 V for 1000 cd m^{-2} and maximum efficiencies of 33.1 and 43.5 lm W^{-1} for blue- and white-emitting devices, respectively, which is the best result reported so far among the prototype low-voltage-driving PHOLEDs. The ultralow operation voltages, high efficiencies, and improved efficiency stability pave the way for the practical applications of these devices in portable displays and lighting. Furthermore, the short-axis substitution effect would guide subsequent investigations and designs, since similar effects may exist in other conjugation systems involving *third and later row* elements. Related work is ongoing in our labatory.

4. EXPERIMENTAL SECTION

4.1. Materials and Instruments. All the reagents and solvents used for synthesis were purchased from Aldrich and Acros companies and used without further purification.

^{1}H NMR spectra were recorded using a Varian Mercury plus 400NB spectrometer relative to tetramethylsilane (TMS) as internal standard. Molecular masses were determined by a Finnigan LCQ electrospray ionization mass spectrometry (ESI-MS), or a MALDI-TOF-MS. Elemental analyses were performed on a Vario EL III elemental analyzer. Absorption and photoluminescence (PL) emission spectra of the target compound were measured using a Shimadzu UV-3150 spectrophotometer and a Shimadzu RF-5301PC spectrophotometer, respectively. Thermogravimetric analysis and differential scanning calorimetry were performed on Shimadzu DSC-60A and DTG-60A thermal analyzers under nitrogen atmosphere at a heating rate of 10 °C min^{-1}. Cyclic voltammetry studies were conducted using an Eco Chemie B.V. AUTOLAB potentiostat in a typical three-electrode cell with a platinum sheet working electrode, a platinum wire counter electrode, and a silver/silver nitrate (Ag/Ag^+) reference electrode. All electrochemical experiments were carried out under a nitrogen atmosphere at room temperature in CH_2Cl_2 for oxidation and tetrahydrofuran (THF) for reduction. Phosphorescence spectra were measured in dichloromethane (DCM) using an Edinburgh FPLS 920 fluorescence spectrophotometer at 77 K cooling by liquid nitrogen with a delay of 300 μs using the time-correlated single photon counting method with a microsecond pulsed xenon light source for 10 μs−10 s lifetime measurement, the synchronization photomultiplier for signal collection and the multichannel scaling mode of the PCS900 fast counter PC plug-in card for data processing. The crystal suitable for single-crystal XRD analysis was obtained through the slow evaporation of the ethanol solution of the compound at room temperature. All diffraction data were collected at 295 K on a Rigaku RAXIS-RAPID diffractometer with graphite monochromatized Mo Kα (λ = 0.71073 Å) radiation in ω scan mode. All structures were solved by direct method and difference Fourier syntheses. Non-hydrogen atoms were refined by full-matrix least-squares techniques on F^2 with anisotropic thermal parameters. The hydrogen atoms attached to carbons were placed in calculated positions with C−H = 0.93 Å and $U(H) = 1.2U_{eq}(C)$ in the riding model approximation. All calculations were carried out with the SHELXL97 program. The thin films of the PO compounds were prepared through vacuum evaporation on glass substrates under the same condition of device fabrication. The morphological characteristics of these films were measured with an Agilent 5100 atom force microscope under the tapping mode and a HITACHI S-4800 scanning electron microscope (spraying; accelerating voltage, 5.0 kV; current, 10 mA; and observed altitude, 8 mm).

4.2. Synthesis. *4-Diphenylphosphoryl Dibenzothiophene (**DBTSPO**).* At −78 °C, a solution of 4.0 mL of *n*-butyllithium (2.5 M in *n*-hexane, 10 mmol) was added dropwise to a stirred solution of 1.8426 g of **DBT** (10 mmol) and 1.51 mL of *N,N,N′,N′*-tetramethylethenyldiamine (10 mmol) in 50 mL of ethyl ether. After all the *n*-butyllithium was added, the cooling bath was removed, and the reaction mixture was warmed to room temperature. After 16 h, the mixture was cooled to −78 °C, and a solution of 1.79 mL of chlorodiphenylphosphine (10 mmol) was added dropwise. The cooling bath was removed, and the reaction mixture was stirred for another 16 h. The reaction was quenched by 10 mL of water, and extracted by DCM (3 × 30 mL). The organic layer was dried with anhydride Na_2SO_4. The solvent was removed *in vacuo*. The residue was dissolved by 50 mL of DCM, 3 mL of hydrogen peroxide (30%)

dx.doi.org/10.1021/ja308273y | J. Am. Chem. Soc. 2012, 134, 19179−19188

was added, and the reaction mixture was stirred for 4 h. The reaction was extracted by sodium hydrogen sulfite-saturated solution. The organic layer was dried with anhydride Na_2SO_4. The solvent was removed *in vacuo*. The residue was purified with flash chromatograph. Yield: 2.3 g of white powder (60%). ^{1}H NMR (400 MHz, $CDCl_3$, TMS): δ (ppm) 8.335 (d, J = 7.2 Hz, 1H, DBT-H); 8.231−8.157 (m, 1H, DBT-H); 7.849−7.720 (m, 5H); 7.591 (t, J = 7.0 Hz, 2H); 7.547−7.431 (m, 8H); LDI-TOF: m/z (%): 384 (100) M^+. Elemental analysis (%) for $C_{24}H_{17}OPS$: C 74.98, H 4.46, O 4.16, S 8.34; found C 75.06, H 4.42, O 4.27, S 8.54.

*4,6-Bis(diphenylphosphoryl) Dibenzothiophene (**DBTDPO**).* This compound was prepared according to the procedure described for **DBTSPO**, but from 1.8426 g of **DBT** (10 mmol) with 3 equiv of *n*-butyllithium and chlorodiphenylphosphine. Yield: 1.75 g of white powder (30%). ^{1}H NMR (400 MHz, $CDCl_3$, TMS): δ (ppm) 8.352 (d, J = 8.0 Hz, 2H); 7.787 (q, J = 6.8 Hz,13.2 Hz, 2H); 7.696−7.622 (m, 8H); 7.602−7.517 (m, 6H) ; 7.472−7.388 (m, 8H); LDI-TOF: m/z (%): 584 (100) M^+. Elemental analysis (%) for $C_{36}H_{26}O_2P_2S$: C 73.96, H 4.48, O 5.47, S 5.48; found C 74.11, H 4.53, O 5.62, S 5.60.

4.3. DFT Calculations. Computations on the electronic ground state and T_1 state of the single-molecular compounds *in vacuo* were performed using Becke's three-parameter density functional in combination with the nonlocal correlation functional of Lee, Yang, and Parr (B3LYP).[61,62] 6-31G(d) basis sets were employed. The ground-state geometries were fully optimized. The fully optimized stationary points were further characterized by harmonic vibrational frequency analysis to ensure that real local minima had been found without imaginary vibrational frequency. All computations were performed using the Gaussian 03 package.[63] The ESP surfaces were visualized with ChemBio3D Ultra 11.0.

4.4. Device Fabrication and Testing. Prior to the device fabrication, the patterned ITO-coated glass substrates were scrubbed and sonicated consecutively with acetone, ethanol, and deionized water, respectively. All the organic layers were thermally deposited in vacuum (~4.0×10^{-4} Pa) at a rate of 1−2 Å/s monitored in situ with the quartz oscillator. In order to reduce the ohmic loss, a heavily p-doped layer with MoO_x, considering the low doping efficiency in amorphous organic matrix with transition-metal-oxide-based acceptors, was directly deposited onto the ITO substrate for each sample. After the deposition of Cs_2CO_3, the samples were transferred to metal chamber, and suffered from a vacuum break due to the change of the shadow masks to determine the active area. The current−voltage−luminance characteristics were measured with a PR650 spectrascan spectrometer and a Keithley 2400 programmable voltage−current source. All the samples were measured directly after fabrication without encapsulation in ambient atmosphere at room temperature.

■ ASSOCIATED CONTENT

Supporting Information

CIF files for single crystals; spin density distribution contours; thermal and morphological analysis results; DFT calculation results of **DBT** analogues; absorption and PL spectra of **DBTSPO** and **DBTDPO** in film and various solvents; PL decay of **DBTSPO** and **DBTDPO** in DCM; device energy level diagram; EL spectra; EL performance of green-, yellow-, and red-emitting devices; and efficiency−J curves of the devices. This material is available free of charge via the Internet at http://pubs.acs.org.

■ AUTHOR INFORMATION

Corresponding Author

hxu@hlju.edu.cn; zhao_yi@jlu.edu.cn

Author Contributions

‡C.H. and Z.Z. contributed equally.

Notes

The authors declare no competing financial interest.

■ ACKNOWLEDGMENTS

This work was financially supported by the National Key Basic Research and Development Program of China (2010CB327701), NSFC (50903028, 61176020 and 60977024), Key Project of Ministry of Education (212039), New Century Talents Developing Program of Heilongjiang Province (1252-NCET-005), Education Bureau of Heilongjiang Province (10td03), and the Supporting Program of Highlevel Talents of HLJU (2010hdtd08).

■ REFERENCES

(1) Peumans, P.; Uchida, S.; Forrest, S. R. *Nature* **2003**, *425*, 158.
(2) Baldo, M. A.; O'Brien, D. F.; You, Y.; Shoustikov, A.; Sibley, S.; Thompson, M. E.; Forrest, S. R. *Nature* **1998**, *395*, 151.
(3) Ma, Y.; Zhang, H.; Shen, J.; Che, C. *Synth. Met.* **1998**, *94*, 245.
(4) Burroughes, J. H.; Bradley, D. D. C.; Brown, A. R.; Marks, R. N.; Mackay, K.; Friend, R. H.; Burns, P. L.; Holmes, A. B. *Nature* **1990**, *347*, 539.
(5) Tang, C. W.; VanSlyke, S. A. *Appl. Phys. Lett.* **1987**, *51*, 913.
(6) Zhao, Q.; Li, F.; Huang, C. *Chem. Soc. Rev.* **2010**, *39*, 3007.
(7) Sun, Y.; Welch, G. C.; Leong, W. L.; Takacs, C. J.; Bazan, G. C.; Heeger, A. J. *Nat. Mater.* **2012**, *11*, 44.
(8) Zhu, X.-H.; Peng, J.; Cao, Y.; Roncali, J. *Chem. Soc. Rev.* **2011**, *40*, 3509.
(9) Xiao, L.; Chen, Z.; Qu, B.; Luo, J.; Kong, S.; Gong, Q.; Kido, J. *Adv. Mater.* **2011**, *23*, 926.
(10) Sasabe, H.; Kido, J. *Chem. Mater.* **2011**, *23*, 621.
(11) Reineke, S.; Lindner, F.; Schwartz, G.; Seidler, N.; Walzer, K.; Lussem, B.; Leo, K. *Nature* **2009**, *459*, 234.
(12) Kamtekar, K. T.; Monkman, A. P.; Bryce, M. R. *Adv. Mater.* **2010**, *22*, 572.
(13) Wei, Y.; Chen, C.-T. *J. Am. Chem. Soc.* **2007**, *129*, 7478.
(14) Qin, T.; Wiedemair, W.; Nau, S.; Trattnig, R.; Sax, S.; Winkler, S.; Vollmer, A.; Koch, N.; Baumgarten, M.; List, E. J. W.; Müllen, K. *J. Am. Chem. Soc.* **2011**, *133*, 1301.
(15) Liao, S.-H.; Shiu, J.-R.; Liu, S.-W.; Yeh, S.-J.; Chen, Y.-H.; Chen, C.-T.; Chow, T. J.; Wu, C.-I. *J. Am. Chem. Soc.* **2008**, *131*, 763.
(16) Lo, M. Y.; Zhen, C.; Lauters, M.; Jabbour, G. E.; Sellinger, A. *J. Am. Chem. Soc.* **2007**, *129*, 5808.
(17) Son, H.-J.; Han, W.-S.; Chun, J.-Y.; Kang, B.-K.; Kwon, S.-N.; Ko, J.; Han, S. J.; Lee, C.; Kim, S. J.; Kang, S. O. *Inorg. Chem.* **2008**, *47*, 5666.
(18) Wang, L.; Jiang, Y.; Luo, J.; Zhou, Y.; Zhou, J.; Wang, J.; Pei, J.; Cao, Y. *Adv. Mater.* **2009**, *21*, 4854.
(19) Lin, S.-L.; Chan, L.-H.; Lee, R.-H.; Yen, M.-Y.; Kuo, W.-J.; Chen, C.-T.; Jeng, R.-J. *Adv. Mater.* **2008**, *20*, 3947.
(20) Rathnayake, H. P.; Cirpan, A.; Delen, Z.; Lahti, P. M.; Karasz, F. E. *Adv. Funct. Mater.* **2007**, *17*, 115.
(21) Li, H.-C.; Lin, Y.-P.; Chou, P.-T.; Cheng, Y.-M.; Liu, R.-S. *Adv. Funct. Mater.* **2007**, *17*, 520.
(22) Lai, W.-Y.; He, Q.-Y.; Zhu, R.; Chen, Q.-Q.; Huang, W. *Adv. Funct. Mater.* **2008**, *18*, 265.
(23) Chen, C.-H.; Huang, W.-S.; Lai, M.-Y.; Tsao, W.-C.; Lin, J. T.; Wu, Y.-H.; Ke, T.-H.; Chen, L.-Y.; Wu, C.-C. *Adv. Funct. Mater.* **2009**, *19*, 2661.
(24) Baldo, M. A.; Lamansky, S.; Burrows, P. E.; Thompson, M. E.; Forrest, S. R. *Appl. Phys. Lett.* **1999**, *75*, 4.
(25) Adachi, C.; Kwong, R. C.; Djurovich, P.; Adamovich, V.; Baldo, M. A.; Thompson, M. E.; Forrest, S. R. *Appl. Phys. Lett.* **2001**, *79*, 2082.
(26) Holmes, R. J.; D'Andrade, B. W.; Forrest, S. R.; Ren, X.; Li, J.; Thompson, M. E. *Appl. Phys. Lett.* **2003**, *83*, 3818.
(27) Holmes, R. J.; Forrest, S. R.; Tung, Y.-J.; Kwong, R. C.; Brown, J. J.; Garon, S.; Thompson, M. E. *Appl. Phys. Lett.* **2003**, *82*, 2422.
(28) Tokito, S.; Iijima, T.; Suzuri, Y.; Kita, H.; Tsuzuki, T.; Sato, F. *Appl. Phys. Lett.* **2003**, *83*, 569.
(29) Tao, Y.; Yang, C.; Qin, J. *Chem. Soc. Rev.* **2011**, *40*, 2943.

(30) Lin, M.-S.; Chi, L.-C.; Chang, H.-W.; Huang, Y.-H.; Tien, K.-C.; Chen, C.-C.; Chang, C.-H.; Wu, C.-C.; Chaskar, A.; Chou, S.-H.; Ting, H.-C.; Wong, K.-T.; Liu, Y.-H.; Chi, Y. *J. Mater. Chem.* **2012**, *22*, 870.
(31) Schrögel, P.; Hoping, M.; Kowalsky, W.; Hunze, A.; Wagenblast, G.; Lennartz, C.; Strohriegl, P. *Chem. Mater.* **2011**, *23*, 4947.
(32) Kim, D.; Coropceanu, V.; Brédas, J.-L. *J. Am. Chem. Soc.* **2011**, *133*, 17895.
(33) Jankus, V.; Monkman, A. P. *Adv. Funct. Mater.* **2011**, *21*, 3350.
(34) Hu, D.; Shen, F.; Liu, H.; Lu, P.; Lv, Y.; Liu, D.; Ma, Y. *Chem. Commun.* **2012**, *48*, 3015.
(35) Su, S. J.; Sasabe, H.; Pu, Y. J.; Nakayama, K.; Kido, J. *Adv. Mater.* **2010**, *22*, 3311.
(36) Fan, C.-H.; Sun, P.; Su, T.-H.; Cheng, C.-H. *Adv. Mater.* **2011**, *23*, 2981.
(37) Yu, D.; Zhao, F.; Han, C.; Xu, H.; Li, J.; Zhang, Z.; Deng, Z.; Ma, D.; Yan, P. *Adv. Mater.* **2012**, *24*, 509.
(38) Zhao, J.; Xie, G.-H.; Yin, C.-R.; Xie, L.-H.; Han, C.-M.; Chen, R.-F.; Xu, H.; Yi, M.-D.; Deng, Z.-P.; Chen, S.-F.; Zhao, Y.; Liu, S.-Y.; Huang, W. *Chem. Mater.* **2011**, *23*, 5331.
(39) Han, C.; Xie, G.; Xu, H.; Zhang, Z.; Yu, D.; Zhao, Y.; Yan, P.; Deng, Z.; Liu, S. *Chem.—Eur. J.* **2011**, *17*, 445.
(40) Han, C.; Xie, G.; Xu, H.; Zhang, Z.; Xie, L.; Zhao, Y.; Liu, S.; Huang, W. *Adv. Mater.* **2011**, *23*, 2491.
(41) Chou, H.-H.; Cheng, C.-H. *Adv. Mater.* **2010**, *22*, 2468.
(42) Hsu, F.-M.; Chien, C.-H.; Shu, C.-F.; Lai, C.-H.; Hsieh, C.-C.; Wang, K.-W.; Chou, P.-T. *Adv. Funct. Mater.* **2009**, *19*, 2834.
(43) Hsu, F.-M.; Chien, C.-H.; Shih, P.-I.; Shu, C.-F. *Chem. Mater.* **2009**, *21*, 1017.
(44) Swensen, J. S.; Polikarpov, E.; Von Ruden, A.; Wang, L.; Sapochak, L. S.; Padmaperuma, A. B. *Adv. Funct. Mater.* **2011**, *21*, 3250.
(45) Han, C.; Xie, G.; Li, J.; Zhang, Z.; Xu, H.; Deng, Z.; Zhao, Y.; Yan, P.; Liu, S. *Chem.—Eur. J.* **2011**, *17*, 8947.
(46) Han, C.; Zhang, Z.; Xu, H.; Li, J.; Xie, G.; Chen, R.; Zhao, Y.; Huang, W. *Angew. Chem., Int. Ed.* **2012**, *51*, 10104.
(47) Jeon, S. O.; Lee, J. Y. *J. Mater. Chem.* **2012**, *22*, 4233.
(48) Padmaperuma, A. B.; Sapochak, L. S.; Burrows, P. E. *Chem. Mater.* **2006**, *18*, 2389.
(49) Vecchi, P. A.; Padmaperuma, A. B.; Qiao, H.; Sapochak, L. S.; Burrows, P. E. *Org. Lett.* **2006**, *8*, 4211.
(50) Jeon, S. O.; Yook, K. S.; Joo, C. W.; Lee, J. Y. *Adv. Funct. Mater.* **2009**, *19*, 3644.
(51) Jang, S. E.; Joo, C. W.; Jeon, S. O.; Yook, K. S.; Lee, J. Y. *Org. Electron.* **2010**, *11*, 1059.
(52) Kim, D.; Salman, S.; Coropceanu, Veaceslav; Salomon, E.; Padmaperuma, A. B.; Sapochak, L. S.; Kahn, A.; Bredas, J.-L. *Chem. Mater.* **2010**, *22*, 247.
(53) Baldo, M. A.; Adachi, C.; Forrest, S. R. *Phys. Rev. B* **2000**, *62*, 10967.
(54) Kalinowski, J.; Stampor, W.; Mecedilzdotyk, J.; Cocchi, M.; Virgili, D.; Fattori, V.; Di Marco, P. *Phys. Rev. B* **2002**, *66*, 235321.
(55) Reineke, S.; Walzer, K.; Leo, K. *Phys. Rev. B* **2007**, *75*, 125328.
(56) Giebink, N. C.; Forrest, S. R. *Phys. Rev. B* **2008**, *77*, 235215.
(57) Sapochak, L.; Padmaperuma, A. B.; Vecchi, P. A.; Cai, X.; Burrows, P. E. *Proc. SPIE* **2007**, *6655*, 665506.
(58) Jeon, S. O.; Yook, K. S.; Joo, C. W.; Lee, J. Y. *Adv. Mater.* **2010**, *22*, 1.
(59) Gilheany, D. G. *Chem. Rev.* **1994**, *94*, 1339.
(60) Gather, M. C.; Koehnen, A.; Meerholz, K. *Adv. Mater.* **2011**, *23*, 233.
(61) Becke, A. D. *J. Chem. Phys.* **1993**, *98*, 5648.
(62) Lee, C.; Yang, W.; Parr, R. G. *Phys. Rev. B* **1988**, *37*, 785.
(63) Frisch, M. J.; Trucks, G. W.; Schlegel, H. B.; Scuseria, G. E.; Robb, M. A.; Cheeseman, J. R.; Montgomery, J. A., Jr.; Kudin, K. N.; Burant, J. C.; Millam, J. M.; Iyengar, S. S.; Tomasi, J.; Barone, V.; Mennucci, B.; Cossi, M.; Scalmani, G.; Rega, N.; Petersson, G. A.; Nakatsuji, H.; Hada, M.; Ehara, M.; Toyota, K.; Fukuda, R.; Hasegawa, J.; Ishida, M.; Nakajima, T.; Honda, Y.; Kitao, O.; Nakai, H.; Klene, M.; Li, X.; Knox, J. E.; Hratchian, H. P.; Cross, J. B.; Adamo, C.; Jaramillo, J.; Gomperts, R.; Stratmann, R. E.; Yazyev, O.; Austin, A. J.; Cammi, R.; Pomelli, C.; Ochterski, J. W.; Ayala, P. Y.; Morokuma, K.; Voth, G. A.; Salvador, P.; Dannenberg, J. J.; Zakrzewski, V. G.; Dapprich, S.; Daniels, A. D.; Strain, M. C.; Farkas, O.; Malick, D. K.; Rabuck, A. D.; Raghavachari, K.; Foresman, J. B.; Ortiz, J. V.; Cui, Q.; Baboul, A. G.; Clifford, S.; Cioslowski, J.; Stefanov, B. B.; G. Liu, A. L.; Piskorz, P.; Komaromi, I.; L.Martin, R.; Fox, D. J.; Keith, T.; Al-Laham, M. A.; Peng, C. Y.; Nanayakkara, A.; Challacombe, M.; Gill, P. M. W.; Johnson, B.; Chen, W.; Wong, M. W.; Gonzalez, C.; Pople, J. A. *Gaussian 03*, Revision D.02; Gaussian Inc.: Pittsburgh, PA, 2004.